Physical Breast Phantom Dedicated for Mammography Studies

Firgan Feradov[1(✉)], Stoyko Marinov[2], and Kristina Bliznakova[1]

[1] Laboratory of Computer Simulations in Medicine, Technical University – Varna, 9010 Varna, Bulgaria
csmlab@tu-varna.bg
[2] Department of Imaging and Pathology, KU Leuven, Herestraat 49, 3000 Leuven, Belgium

Abstract. This paper presents a simple methodology for creation of anthropomorphic physical breast phantoms dedicated for x-ray breast imaging. The use of physical phantoms in diagnostic radiology is a well-established approach for patient dose estimation, quality control of developed diagnostic systems and development of new breast imaging techniques. An overview of the design process used for the creation of the presented phantom and evaluation approach is given. A combination of materials (Clear resin, Gray resin and PLA) and methods (fused deposition modelling and stereolithography) are used for the manufacturing of the breast phantom. The phantom was subjected to an evaluation aiming at its suitability for studies with digital mammography technique. In particular, the created phantom was evaluated by using two sets of phantom images, taken using 22 kVp and 28 kVp, which are compared with real mammograms. The comparison of the images is based on extracted statistical parameters – namely skewness, kurtosis, fractals, PSA, GLCMContrast and GLCMEnergy.

Keywords: Physical breast phantom · Suitable materials · Evaluation

1 Introduction

Nowadays the use of breast physical phantoms is related to the applications in diagnostic radiology related to optimization of patient dose, quality control of developed diagnostic systems (Breast Tomosynthesis, breast CT, contrast-enhanced mammography units), as well as for proof of concept and development of new breast imaging techniques [1, 2]. Until recently, the exploited phantoms in the routine clinical work were mainly represented by a homogeneous mixture, incorporating standard test objects dedicated for system performance evaluation.

Recent advanced research in the field of 3D printing materials and technology for printing phantoms dedicated to x-ray breast imaging showed the attempts to produce realistic anthropomorphic breast phantoms from patient images [3] and computational breast models [4]. These are also used in education approach for teaching purposes at advanced classes. An example is the advanced educational course in Medical Physics at European level EUTEMPE-RX, where at several modules the participants are trained to perform virtual studies with anthropomorphic phantoms [5–8].

J. Henriques et al. (Eds.): MEDICON 2019, IFMBE Proceedings 76, pp. 344–352, 2020.
https://doi.org/10.1007/978-3-030-31635-8_41

One major problem with the 3D printing approach is related to the limitations in the current 3D technology, which, however, has made enormous progress during the last two years in terms of technology and materials focused on printing 3D anthropomorphic phantoms. For example, phantoms may now be printed by using inexpensive parchment paper and a radiopaque ink [9].

We have recently studied the absorption and phase-contrast characteristics of several materials commonly used with fuse deposition modelling and stereolithography 3D printers [10, 11]. These studies showed that most of the resins, Nylon, Hybrid, PET-G have absorption properties in the mammography range similar to these of the glandular tissue, while ABS shows absorption characteristics close to these of the adipose tissue. Based on these findings, we further developed a physical phantom, based on these materials. This paper reports on the process, related to the manufacturing of such phantoms and its evaluation for mammography purposes. The evaluated phantoms will be used for assessment of new breast imaging techniques such as phase contrast mammography.

2 Materials and Methods

2.1 Physical Breast Phantom

The main elements in manufacturing a physical breast phantom are depicted in Fig. 1a, while Fig. 1b shows the complete phantom, filled with water. Specifically, the external shape is a semi-cylinder container with sizes: radius of the semi-cylinder base 59 mm, and 49 mm height.

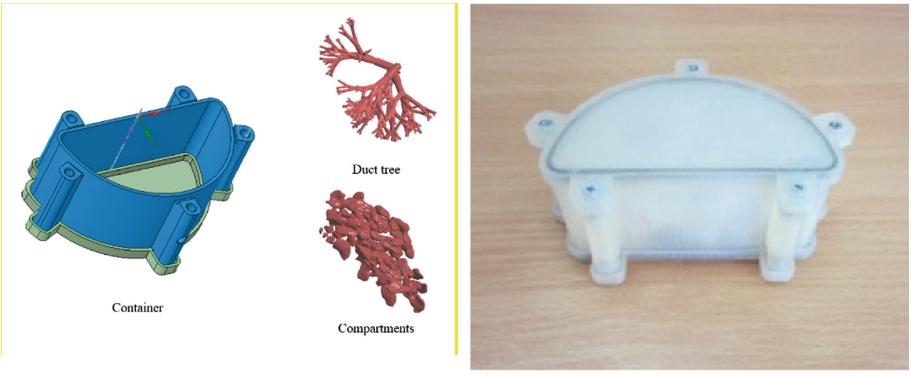

(a) (b)

Fig. 1. Physical breast phantom: (a) main parts, (b) the manufactured physical breast phantom

Two 3D printing technologies are used: fused deposition modelling (FDM) and stereolithography (SLA). The materials used for the production of the phantom are summarized in Table 1. Their properties are taken from Ivanov et al. [10].

Table 1. Materials used for manufacturing of the breast phantom.

Phantom element	Elemental composition						Technology
	Material	H	C	N	O	Density g/cm^3	
Glandular tree	Clear	0.085	0.648	0.059	0.208	1.180	SLA
Adipose compartments	Gray	0.084	0.638	0.052	0.226	1.175	SLA
Skin	PLA	0.058	0.541	0.018	0.383	1.250	FDM

The semicylinder container was modelled with the help of DesignSpark Mechanical 2.0 (https://www.rs-online.com/designspark/mechanical-software), while the glandular tree is modelled with the BreastSimulator [12, 13]. The adipose compartments were based on segmented adipose models from tomography images of the breast [14, 15]. As there are no requirements for breast phantoms to contain pathology, the inclusion of such was not considered at this stage of the development process.

2.2 Experimental Setup

X-ray images of the physical phantom shown in Fig. 1 were acquired with a Siemens digital mammography unit featuring a detector with a pixel size of 0.085 mm $\times$ 0.085 mm. Two projection sets, each one comprising of ten images, were taken at tube voltages set to 22 kVp and 28 kVp, respectively. Two such mammography images are shown in Fig. 2.

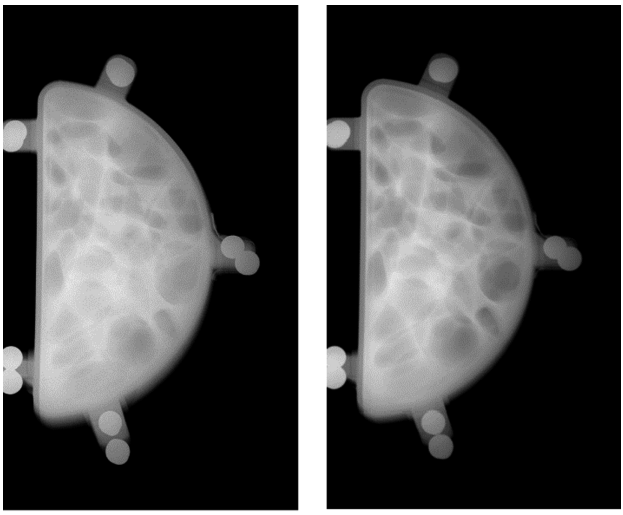

(a) (b)

Fig. 2. Mammography images of the phantom shown in Fig. 1b acquired with (a) 22 kVp (b) 28 kVp.

The source to detector distance was 660 mm, while the incident exposure depended from the phantom thickness.

2.3 Evaluation

The evaluation has been carried out with an in-house developed tool dedicated for feature extraction from x-ray images [16]. Figure 3 shows the main window of the tool. The user interface is implemented in MATLAB 2013a environment using the GUIDE module [17]. In short, the tool is divided into five regions related to different activities and functionalities, such as (a) various possibilities to load DICOM and other types of images, (b) possibilities to adjust contrast and brightness by using sliders, to zoom in/out the image and examine the details of specific pixel, (c) functionalities related to manually or automatically defining the regions of interest (ROI) in the selected image, (d) use of tools for automatic creation of 'mask' image of the area of the breast, where the ROIs are populated, (e) calculation of features based on the selected ROIs.

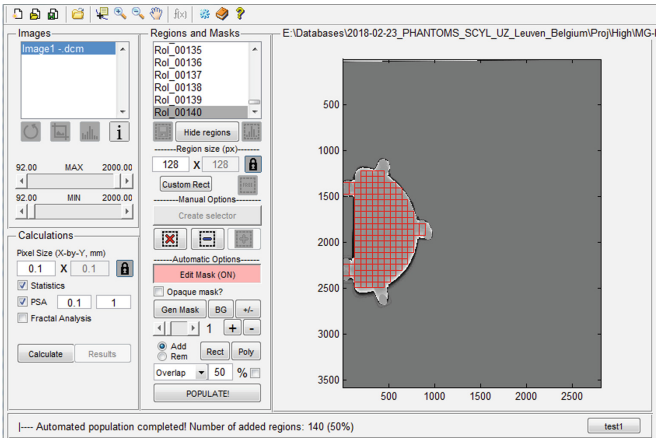

Fig. 3. A screenshot of the main window of the tool, used in the evaluation.

Texture of a breast in mammogram images plays significant role in tissue classifications. This tool is capable of evaluating more than 20 statistical and other feature types. In this study, we used six features of interest, which description is shortly summarized in Table 2.

The evaluation of the phantom has been performed by comparison of features extracted from x-ray mammography images compared to those extracted from 20 mammography patient images. The described features are performed over randomly selected ROIs in the analyzed images and further averaged and expressed by a mean value and standard deviation.

Table 2. Feature description.

Kurtosis. It expresses the relative tailedness, relatively to the Gaussian distribution or flatness of the distribution of the image pixel values:

$$\mathrm{Kurt}[X] = \frac{\mu_4}{\sigma^4} = \frac{E[(X-\mu)^4]}{(E[(X-\mu)^2])^2} \quad [1]$$

where E is the expectation operator, μ_4 is the fourth moment about the mean (μ) and σ is the standard deviation.

Kurtosis is used for evaluation of the local structural texture. Higher values of kurtosis (positive) signify absence of local extreme values and vice versa – which is connected to the homogeneity of the texture and the breast density.

Skewness. It describes the asymmetry of the probability distribution of the image pixel values about their mean. The skewness value can be positive or negative, or undefined.

$$\gamma_1 = \mathrm{E}\left[\left(\frac{X-\mu}{\sigma}\right)^3\right] = \frac{\mu_3}{\sigma^3} = \frac{E[(X-\mu)^3]}{(E[(X-\mu)^2])^{\frac{3}{2}}} = \frac{\kappa_3}{\kappa_2^{3/2}} \quad [2]$$

where E is the expectation operator, μ_3 is the third central moment.

This descriptor is used for evaluation of the density of the breast: negative skewness is a sign of fibroglandular tissue, while positive skewness is a characteristic of the fatty tissue.

Fractal Analysis. Computes fractal characteristics of the images, which can be used to describe the smoothness/roughness of the image intensity. The area A(ε) of each image pixel and its difference (treated us surface) with the neighboring pixels right of and below it is computed according to:

$$A(\varepsilon) = \sum_{x,y} \varepsilon^2 + \sum_{x,y} \varepsilon(|i_\varepsilon(x,y) - i_\varepsilon(x,y+1)| + |i_\varepsilon(x,y) - i_\varepsilon(x+1,y)|) \quad [3]$$

The fractal dimension D of an image is then calculated as:

$$D = 2 - \frac{\Delta \log[A(\varepsilon)]}{\Delta \log[\varepsilon]} \quad [4]$$

This descriptor is used for evaluation of the degree of complexity of the breast's textural patterns – low fractal dimensional value implies a simple homogeneous texture/structure.

Power law spectral analysis (PSA). The power spectrum describes the signal and noise into frequency components of which the low frequency range can be characterized by following a power law. The exponent of this power law is a measure of the texture or anatomical clutter.

$$F(k,l) = \frac{1}{MN} \sum_{a=0}^{M-1} \sum_{b=0}^{N-1} f(a,b) \exp\left[-2\pi i \left(\frac{ka}{M} + \frac{lb}{N}\right)\right] \quad [5]$$

where k (0, 1..., M−1) and l (0, 1,…, N−1) are the relative spatial frequencies in the two directions and M×N is the image size in pixels. The power spectrum profile is given by:

$$|S0(f)|^2 \approx \frac{c}{f^{2\beta}} \quad [6]$$

where f is a radial frequency variable, and c is a constant. The logarithm to base 2 of the total power spectrum is further plotted versus the octave number. The trend is almost linear and the data are fitted to a line obtained using linear regression analysis. The slope of the line m is related to the exponential parameter β as: $m = \beta - 2$.

This descriptor is used for evaluation of the breast's density.

(*continued*)

Table 2. (*continued*)

GLCM (Gray-level co-ocurrence matrix) Energy. Returns the sum of squared elements in the GLCM. The *Energy* is also known as uniformity, uniformity of energy, and angular second moment and is calculated as: $$F_{GLCM\ Energy} = \sum_{i=1}^{N_0}\sum_{j=1}^{N_0} p_{ij}^2 \quad [7]$$ where p_{ij} is the probability value for the ij-th gray tone from the calculated GLCM matrix. **This descriptor is used for evaluation of the structural patterns throughout the whole texture.**
GLCM Contrast. Returns a measure of the intensity contrast between a pixel and its neighbor over the whole image. *Contrast* is known as variance and inertia and is calculated as: $$F_{GLCM\ Contrast} = \sum_{i=1}^{N_0}\sum_{j=1}^{N_0}(i-j)^2 p_{ij} \quad [8]$$ **This descriptor is used for evaluation of the local variations throughout the texture.**

3 Results and Discussion

For the calculations of the features, we used ROIs of size 128 × 128 pixels and 50% overlap of the regions. All ROIs are placed "inside" the projected breast, excluding skin, muscle and background. Table 3 summarizes the results for the calculated features for each set of ten images, acquired at 28 kVp and 22 kVp, respectively in comparison to the features extracted from twenty patient mammography images, free of lesions.

Table 3. Comparison of features extracted from phantom and patient images.

Descriptor	Physical phantom 28 kVp	Physical phantom 22 kVp	Mammography images
Kurtosis	3.62 ± 2.88	3.58 ± 0.37	3.05 ± 0.07
Skewness	0.48 ± 0.32	0.41 ± 0.06	0.008 ± 0.10
Fractal	3.08 ± 0.04	3.42 ± 0.01	3.07 ± 0.12
PSA	3.08 ± 0.05	2.78 ± 0.08	2.78 ± 0.17
GLCM Contrast	0.79 ± 0.07	1.10 ± 0.04	0.72 ± 0.21
GLCM Energy	0.11 ± 0.03	0.09 ± 0.01	0.10 ± 0.01

The comparison of features shows a good coincidence between features from phantom and patient images. Better agreement is observed for the phantom images obtained with 28 kVp, which is expected since this energy is traditionally used with mammography units. In addition, comparison of distributions of selected features is shown in Fig. 4a–c.

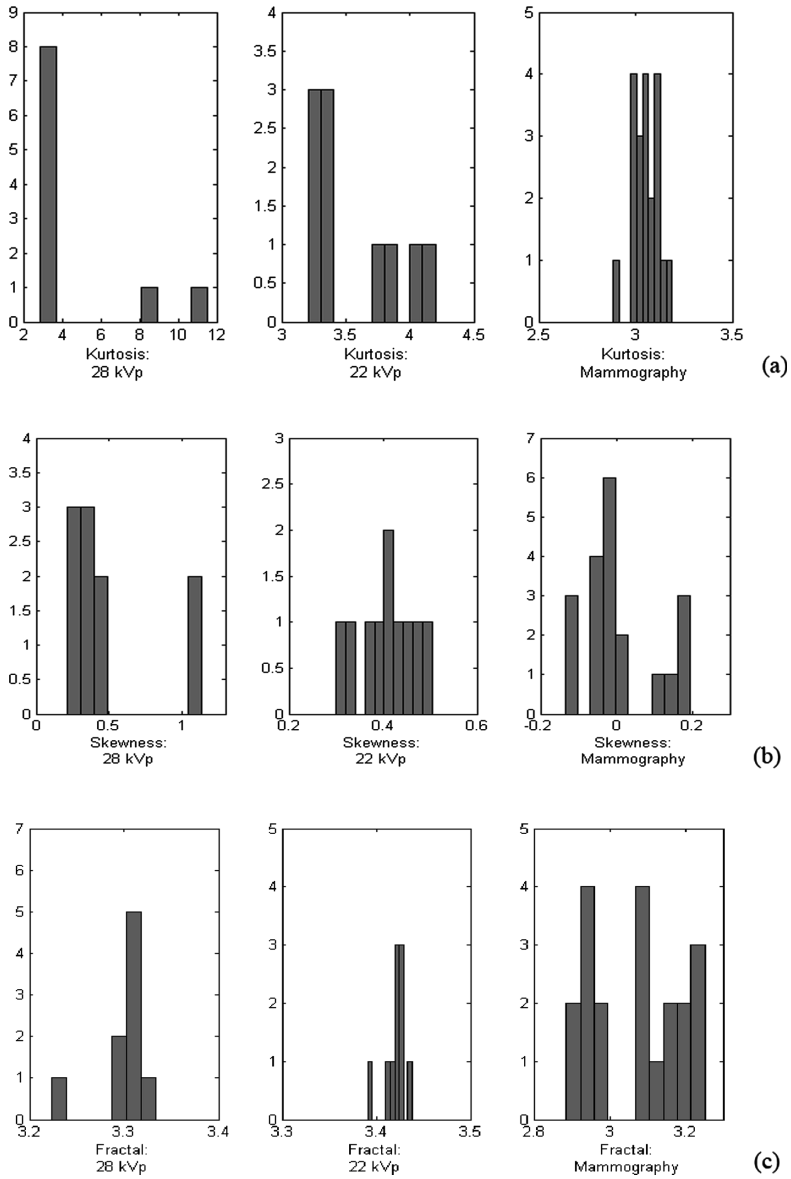

Fig. 4. Distributions of the computed (a) kurtosis, (b), skewness and (c) fractal dimension distributions for the studied images.

4 Conclusions

The conducted comparative evaluation the created physical phantom and the patient mammograms shows similarity between features extracted from their mammography images. From the studied features extracted from mammography images obtained from the two phantom sets of images (taken at 22 kVp and 28 kVp), the use of 28 kVp with the proposed phantom - glandular tree, printed from Gray resin; Adipose compartments, printed from Clear resin and container, printed from PLA - showed close results to these from patient mammography images.

Acknowledgements. This research is supported by the Bulgarian National Science Fund under grant agreement DN17/2.

References

1. Tomal, A., Costa, P.R.: Chapter 56: Phantoms for image quality and dose assessment. In: Russo, P. (ed.) Handbook of X-ray Imaging: Physics and Technology, pp. 1135–1158. CRC Press, Boca Raton (2018)
2. Bliznakova, K.: Chapter 57: Software phantoms for x-ray radiography and tomography. In: Russo, P. (ed.) Handbook of X-ray Imaging: Physics and Technology, pp. 1159–1184. CRC Press, Boca Raton 2018
3. Kiarashi, N., Nolte, A.C., Sturgeon, G.M., Segars, W.P., Ghate, S.V., Nolte, L.W., Samei, E., Lo, J.Y.: Development of realistic physical breast phantoms matched to virtual breast phantoms based on human subject data. Med. Phys. **42**, 4116–4126 (2015)
4. Carton, A.K., Bakic, P., Ullberg, C., Derand, H., Maidment, A.D.: Development of a physical 3D anthropomorphic breast phantom. Med. Phys. **38**, 891–896 (2011)
5. Bosmans, H., Bliznakova, K., Padovani, R., et al.: Eutempe-RX: a new EC supported course for medical physics experts in radiology. Phys. Medica **30**(Supplement 1), e11 (2014)
6. Bosmans, H., Bliznakova, K., Padovani, R., et al.: EUTEMPE-RX, an EC supported FP7 project for the training and education of medical physics experts in radiology. Radiat. Prot. Dosimetry. **165**, 518–522 (2015)
7. Bliznakova, K., Buliev, I., Bosmans, H., et al.: How can biomedical engineers benefit from the new expert level course of the EUTEMPE-RX project. In: 6th European Conference of the International Federation for Medical and Biological Engineering, vol. 45, pp. 765–768 (2015)
8. Bliznakova, K.: Development of breast software phantom dedicated for research and educational purposes. Radiat. Appl. Phys. Chem. Biol. Med. Sci. Eng. Environ. Sci. **2**, 14–19 (2016)
9. Ikejimba, L.C., Graff, C.G., Rosenthal, S., et al.: A novel physical anthropomorphic breast phantom for 2D and 3D x-ray imaging. Med. Phys. **44**, 407–416 (2017)
10. Ivanov, D., Bliznakova, K., Buliev, I., et al.: Suitability of low density materials for 3D printing of physical breast phantoms. Phys. Med. Biol. **63**, 175020 (2018)
11. Esposito, G., Mettivier, G., Bliznakova, K., et al.: Investigation of the refractive index decrement of 3D printing materials for manufacturing breast phantoms for phase contrast imaging. Phys. Med. Biol. **64** (2019)

12. Bliznakova, K., Suryanarayanan, S., Karellas, A., Pallikarakis, N.: Evaluation of an improved algorithm for producing realistic 3D breast software phantoms: application for mammography. Med. Phys. **37**, 5604–5617 (2010)
13. Bliznakova, K., Sechopoulos, I., Buliev, I., Pallikarakis, N.: BreastSimulator: a software platform for breast x-ray imaging research. J. Biomed. Graph. Comput. **2**, 1–14 (2012)
14. Imran, A.A.Z., Bakic, P.R., Pokrajac, D.D.: Spatial distribution of adipose compartments size, shape and orientation in a CT breast image of a mastectomy specimen. In: 2015 IEEE Signal Processing in Medicine and Biology Symposium - Proceedings (2015)
15. Imran, A.A., Pokrajac, D.D., Maidment, A.D.A., Bakic, P.R.: Estimation of adipose compartment volumes in CT images of a mastectomy specimen. In: Medical Imaging 2016: Physics of Medical Imaging, vol. 9783 (2016)
16. Marinov, S., Buliev, I., Cockmartin, L., et al.: Development of a software tool for evaluation of x-ray images: a case study in breast imaging. In: World Congress on Medical Physics and Biomedical Engineering, IUPESMPrague, p. 218, 3–8 June 2018
17. MathWorks: Matlab-MathWorks (2016)